AIAA JOURNAL
Vol. 36, No. 4, April 1998

Modeling of Microcrack Damaged Composite Plates Undergoing Nonlinear Bimodular Flutter Oscillations

Taehyoun Kim,* Satya N. Atluri,† and Robert G. Loewy‡
Georgia Institute of Technology, Atlanta, Georgia 30332-0356

Numerical methods to investigate the flutter response and aeroelastic stability of plates made of composite materials, wherein microcracking occurs in the matrix material, are presented. The analytical modeling of the modulus reduction due to microcracks is based on a self-consistent method with a two-phase model and yields reduced moduli of the composites as functions of the crack density distribution. Both a finite difference and a finite element formulation are presented for two-dimensional laminated plates in supersonic flow. From the numerical results, it is shown that the microcracking in composites results in a loss of aeroelastic stability through nonlinear bimodular oscillation as well as by a direct reduction in the bending stiffness. For three-dimensional flutter problems, however, reduction in the torsional rigidity and changes in elastic couplings may further decrease the stability.

Nomenclature

A_{ij} = laminate extension moduli as defined by Eq. (14)
B_{ij} = laminate coupling moduli as defined by Eq. (15)
D_{ij} = laminate bending moduli as defined by Eq. (16)
L_{ij} = uniply moduli
M = number of finite elements
M_{ij} = uniply compliances
M^0_{ij} = uncracked uniply compliances
M_∞ = Mach number
N = number of plies
t = ply thickness or time
U_∞ = air velocity
u = longitudinal displacement
w = lateral displacement
x = longitudinal coordinate
$z^{(k)}$ = vertical distance from the midplane to the top of the kth ply
z_n = neutral surface location
α = parameter in Newmark's scheme
β = crack density or a parameter in Newmark's scheme
Δp = aerodynamic pressure differential across panel
ϵ_{ij} = in-plane strain components in the laminate axes
$\tilde{\epsilon}_{ij}$ = in-plane strain components in the ply axes
ϵ_0 = total in-plane strain vector at the midplane
κ = total curvature vector
λ = dynamic pressure or a parameter in Newmark's scheme
v_f, v_m = volume fractions of fiber and matrix materials, respectively
ρ_∞ = air density
σ_{ij} = in-plane stress components in the laminate axes
$\tilde{\sigma}_{ij}$ = in-plane stress components in the ply axes

I. Introduction

ALTHOUGH aerospace structures are making greater use of advanced filamentary composite materials than ever before, virtually all of the composites in current use are designed to carry the major loads in fibers. That is, matrix material is left largely unloaded. Just how little load appears in the matrix material depends, of course, on the relative moduli of fibers and matrices. Nevertheless, the integrity of the matrix material plays an important structural role of transferring tensile loads around imperfections or damage in an individual fiber reinforcement and shear transfer from one ply to another. In particular, high transverse shear flexibilities may result in intolerable decay of vibration and flutter performances.[1] Further, composites designed and used so as to have no major loads in the matrix material cannot provide elastic coupling, and there is widespread agreement that elastic coupling can have substantial benefits.[2–5] Elastic couplings, in general, require loading the matrix material in composite laminates.

As described by Hill,[6] microcracks are responsible for variations in the properties (primarily stiffness) of the constituent matrix materials. Composite laminates may develop these cracks at load levels well below the failure load under cyclic or monotonic loading conditions. There has been ample research in the development of theories for solids with microcracks.[6–12] Budiansky and O'Connell[7] developed the self-consistent model to determine the elastic moduli of isotropic solids with cracks. Laws et al.[8] and Dvorak et al.[9] applied this model to calculate reduced moduli of a cracked orthotropic uniply.

The analysis of a microcracked uniply has been used to predict the effect of the damage on the performance of a composite structure. In a series of papers, Makins and Adali[13] and Adali and Makins[14,15] used the theory developed in Refs. 8 and 9 to predict the behavior of cracked laminates in classical plate problems of bending deformation, buckling, and vibration. However, an important feature in the deformation of microcracked laminates, i.e., nonlinear bimodular deformation, was not identified during the course of those studies. The investigation of the frequency characteristics was also limited to cross-ply laminates and therefore did not include effects on elastic couplings. Whereas microcracking in the matrix may have a minor effect on the overall elastic properties of the composite structures, the effects on the aeroelastic moduli of structures, particularly those tailored to provide elastic coupling, can be substantial. To the authors' knowledge, there has been no work reported to this date that properly addresses such issues as they affect the vibration and flutter of microcracked laminates.

The objectives of this paper are to identify and to elucidate the new nonlinear dynamic phenomenon that arises with microcracked laminated composites and thereby to provide a groundwork for investigation of the effects of transverse microcracks in the matrix on the dynamic and aeroelastic behavior of laminated composite structures.

II. Modeling of Microcracks in a Uniply

In a composite laminate, each layer may contain a system of aligned slit cracks that grow in the direction of fibers and through

Received June 16, 1995; revision received Oct. 25, 1997; accepted for publication Nov. 10, 1997.

*Research Scientist, Computational Mechanics Center; currently Senior Specialist Engineer, Aeroelastic Analysis, Boeing Commercial Airplane Group, P.O. Box 3707, MS 67-HM, Seattle, WA 98124-2207. Member AIAA.

†Institute Professor and Regents' Professor of Engineering, Computational Mechanics Center. Fellow AIAA.

‡Professor and Chair, School of Aerospace Engineering. Honorary Fellow AIAA.

the thickness of the ply, perpendicularto the ply's plane. The extent of damage is characterized by the formation of new cracks, not by the growth of existing cracks. The formation of microcracks in a ply reduces the stiffness of the ply and, therefore, changes the overall behavior of the laminate. One way to characterize the crack density of a unidirectionalply is by the parameter $\beta = t/s$, where t is the ply thickness and s the length between cracks in that ply, assuming that the crack distribution is uniform (Fig. 1). Laws et al.[8] and Dvorak et al.[9] proposed an analytical modeling of the microcrack in a uniply, and it will be the basis of our modeling of microcracked composite laminates.

Depending on the fiber diameter relative to an effective medium, one can have either a three-phase or a two-phase model. It is generally known that the predictions of the two models are indistinguishable for most fiber-reinforced composites where the fiber diameter is much smaller than the crack length.[8] According to the two-phase model, the overall stiffness and compliance matrices are given by

$$\boldsymbol{\sigma} = \boldsymbol{L}\boldsymbol{\epsilon}, \qquad \boldsymbol{\epsilon} = \boldsymbol{M}\boldsymbol{\sigma} \tag{1}$$

where

$$\boldsymbol{L} = \boldsymbol{L}_0 - \bar{\beta}\,\boldsymbol{L}_0\,\boldsymbol{\Lambda}\boldsymbol{L} \tag{2}$$

$$\boldsymbol{M} = \boldsymbol{M}_0 + \bar{\beta}\,\boldsymbol{\Lambda} \tag{3}$$

$$\bar{\beta} = \tfrac{1}{4}\,\pi\beta \tag{4}$$

The subscript 0 is used to denote the properties of the uncracked composite. The matrix $\boldsymbol{\Lambda}$ has only three nonzero components:

$$\Lambda_{22} = \frac{M_{11}M_{22} - M_{12}^2}{M_{11}}\left(\alpha_1^{\frac{1}{2}} + \alpha_2^{\frac{1}{2}}\right) \tag{5}$$

$$\Lambda_{44} = \frac{\sqrt{M_{11}\,M_{22} - M_{12}^2}\sqrt{M_{11}\,M_{33} - M_{13}^2}}{M_{11}}\left(\alpha_1^{\frac{1}{2}} + \alpha_2^{\frac{1}{2}}\right) \tag{6}$$

$$\Lambda_{66} = \sqrt{M_{55}\,M_{66}} \tag{7}$$

where α_1 and α_2 are the roots of the quadratic equation

$$\left(M_{11}M_{22} - M_{12}^2\right)\alpha^2 - [M_{11}M_{44} + 2(M_{11}M_{13} - M_{12}M_{13})]\alpha + M_{11}M_{33} - M_{13}^2 = 0 \tag{8}$$

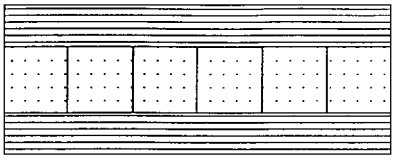

a) No load

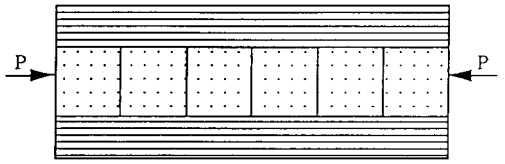

b) Compressive (cracks closed)

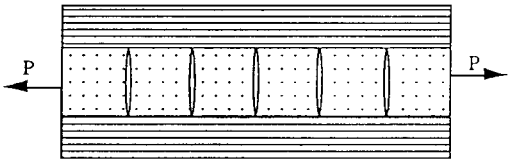

c) Tensile (cracks open)

Fig. 1 Nonlinear behavior of a microcracked ply.

Thus, only three compliance coefficients, M_{22}, M_{44}, and M_{66}, are affected by the presence of microcracks, and the remaining coefficients in $\boldsymbol{M}$ are unchanged from their uncracked properties:

$$M_{22} = M_{22}^0 + \bar{\beta}\,\frac{\left(M_{11}M_{22} - M_{12}^2\right)\left(\alpha_1^{\frac{1}{2}} + \alpha_2^{\frac{1}{2}}\right)}{M_{11}} \tag{9}$$

$$M_{44} = M_{44}^0 + \bar{\beta} \times \frac{\sqrt{M_{11}M_{22} - M_{12}^2}\sqrt{M_{11}M_{33} - M_{13}^2}\left(\alpha_1^{\frac{1}{2}} + \alpha_2^{\frac{1}{2}}\right)}{M_{11}} \tag{10}$$

$$M_{66} = M_{66}^0 + \bar{\beta}\sqrt{M_{55}\,M_{66}} \tag{11}$$

The numerical evaluation of $\boldsymbol{M}$ is achieved by performing an iteration method on the preceding equations beginning with $\boldsymbol{M}^{(1)} = \boldsymbol{M}_0$ (Ref. 9). Once the cracked compliance $\boldsymbol{M}$ is evaluated, the cracked stiffness can be obtained by $\boldsymbol{L} = \boldsymbol{M}^{-1}$.

The preceding analysis applies only to cases wherein the cracks remain open. When the microcracks are closed, the quantification of the reduced stiffness may be nontrivial.[16] In particular, the stiffness matrix does not remain symmetric if slip occurs on crack surfaces. For simplicity, we will assume that the stiffness of a uniply with closed microcracks is equivalent to that of uncracked ply.

III. Calculation of Reduced Laminate Stiffness

A. Overall Laminate Stiffness

For a cracked uniply, the full constitutive equation is

$$\begin{bmatrix}\sigma_{11}\\ \sigma_{22}\\ \sigma_{33}\\ \sigma_{23}\\ \sigma_{13}\\ \sigma_{12}\end{bmatrix} = \begin{bmatrix} L_{11} & L_{12} & L_{13} & 0 & 0 & 0\\ & L_{22} & L_{23} & 0 & 0 & 0\\ & & L_{33} & 0 & 0 & 0\\ & & & L_{44} & 0 & 0\\ & & \text{(Symm)} & & L_{55} & 0\\ & & & & & L_{66}\end{bmatrix}\begin{bmatrix}\epsilon_{11}\\ \epsilon_{22}\\ \epsilon_{33}\\ \gamma_{23}\\ \gamma_{13}\\ \gamma_{12}\end{bmatrix} \tag{12}$$

In the general analysis of laminated composites, including vibration and flutter, it is often adequate to rely on the two-dimensional stress–strain relations based on the classical laminate plate theory (CLPT).[17] According to the CLPT, the force resultant-strain relations for a full composite consisting of N plies are

$$\begin{Bmatrix}\boldsymbol{N}\\ \boldsymbol{M}\end{Bmatrix} = \begin{bmatrix}\boldsymbol{A}(z_n) & \boldsymbol{B}(z_n)\\ \boldsymbol{B}(z_n) & \boldsymbol{D}(z_n)\end{bmatrix}\begin{Bmatrix}\boldsymbol{\epsilon}_0\\ \boldsymbol{\kappa}\end{Bmatrix} \tag{13}$$

where

$$A_{ij}(z_n) = \sum_{k=1}^{N}\int_{z^{(k+1)}}^{z^{(k)}} L_{ij}^{(k)}\,\mathrm{d}z \tag{14}$$

$$B_{ij}(z_n) = \sum_{k=1}^{N}\int_{z^{(k+1)}}^{z^{(k)}} L_{ij}^{(k)}\,z\,\mathrm{d}z \tag{15}$$

$$D_{ij}(z_n) = \sum_{k=1}^{N}\int_{z^{(k+1)}}^{z^{(k)}} L_{ij}^{(k)}\,z^2\,\mathrm{d}z \tag{16}$$

and

$$\boldsymbol{\epsilon}_0 = [\epsilon_{011} \quad \epsilon_{022} \quad \gamma_{012}]^T \tag{17}$$

$$\boldsymbol{\kappa} = [\kappa_{11} \quad \kappa_{22} \quad \kappa_{12}]^T \tag{18}$$

Once microcracks are formed, some of the nonzero entries of the stiffness matrices $\boldsymbol{A}$, $\boldsymbol{B}$, and $\boldsymbol{D}$, particularly those representing elastic coupling terms, will change from their original magnitudes. Further, new coupling terms, such as bending-extension, that did not exist previously may now be present.

The neutral plane position z_n is defined by the equation

$$\epsilon_{11}(z = z_n) = \epsilon_{110} + z_n\,\kappa_{11} = 0 \tag{19}$$

For a two-dimensional plate with flexural bending M_{11} and in-plane axial load N_{11},

$$z_n = \frac{B_{11}\,M_{11} - D_{11}\,N_{11}}{A_{11}\,M_{11} - B_{11}\,N_{11}} \tag{20}$$

It is probably obvious that, in many cases, $\boldsymbol{A}$, $\boldsymbol{B}$, and $\boldsymbol{D}$ are independent of the neutral plane position of the cracked laminate. This is because all of the open cracks are likely to be on either side of the neutral axis. Exceptions would be cases where the laminate is loaded by in-plane forces as well as out-of-plane moments, closing only a portion of the cracked zone. In this case, the through-thickness integrations are taken only over the open portion of the cracked plies with the reduced L_{ij}, and the remaining portion is integrated with L^0_{ij}. Evaluation of this new stiffness becomes a nonlinear procedure because the location of the neutral axis itself depends on the true stiffness. In this paper, to simplify our problem, we deal exclusively with simply supported laminates that are free of in-plane load.

B. Crack-Opening Criterion

In accordance with our earlier assumption, cracked plies in compression (Fig. 1b) behave as though they are uncracked ($\beta = 0$), and those under tension (Fig. 1c) behave according to the crack models. Ultimately, local strain averages at the sites of the cracks will determine the crack opening or closure. In this paper, we adopt the criterion for crack opening or closure as follows: For a cracked ply with index number k and fiber angle $\theta^{(k)}$, cracks will open if

$$\tilde{\epsilon}^{c\,(k)}_{22} > 0$$

and will close if

$$\tilde{\epsilon}^{c\,(k)}_{22} < 0$$

Here, $\tilde{\epsilon}^{c\,(k)}_{22}$ represents the portion of the total strain $\tilde{\epsilon}^{(k)}_{22}$ in the direction normal to the fiber axis that is accommodated by the cracks. The other portion of the total strain is then the average strain of the composite matrix that does not contain any cracks. It can be shown that[9]

$$\tilde{\epsilon}^{c\,(k)}_{22} = \bar{\beta}\Lambda_{22}\left[L^{(k)}_{12}\,\tilde{\epsilon}^{(k)}_{11} + L^{(k)}_{22}\,\tilde{\epsilon}^{(k)}_{22} + L^{(k)}_{23}\,\tilde{\epsilon}^{(k)}_{33}\right] \tag{21}$$

where $\tilde{\epsilon}^{(k)}_{\alpha\beta}$ are the total average strains along the material principal axes of the kth ply. Note that, by a coordinate transformation,

$$\tilde{\epsilon}^{(k)}_{\alpha\beta} = l^{(k)}_{\tilde{\alpha}\gamma}\,l^{(k)}_{\tilde{\beta}\delta}\,\epsilon^{(k)}_{\gamma\delta} \tag{22}$$

where

$$\epsilon^{(k)}_{\gamma\delta} = \epsilon^{(k)}_{0\gamma\delta} + z^{(k)}\,\kappa_{\gamma\delta} \tag{23}$$

are the total strain components along the laminate axes and $l^{(k)}_{\tilde{\alpha}\gamma}\,l^{(k)}_{\tilde{\beta}\delta}$ are the associated direction cosines. In conjunction with the CLPT, Eq. (21) becomes

$$\tilde{\epsilon}^{c\,(k)}_{22} = \bar{\beta}\Lambda_{22}\left\{\left[L^{(k)}_{12} - L^{(k)}_{23}\frac{L^{(k)}_{13}}{L^{(k)}_{33}}\right]\tilde{\epsilon}^{(k)}_{11} + \left[L^{(k)}_{22} - \frac{L^{(k)^2}_{23}}{L^{(k)}_{33}}\right]\tilde{\epsilon}^{(k)}_{22}\right\} \tag{24}$$

where $M^{(k)}_{ij}$ are the elements of uniply compliance matrix for the kth ply.

IV. Nonlinear Bimodular Deformation

In reality, the true distribution of microcracks can be estimated only by static fracture analysis such as given in Ref. 12. The characteristic load to which the laminate is subjected will then determine the degree and locations of the microcracks inside the laminate. In case of a lifting wing or a panel, the structures are frequently loaded by static bending, making their tension sides prone to microcracking. Therefore, without loss of generality, we will assume that all cracks exist on either half side of the cross section. Figure 2a shows a composite plate consisting of a cross-ply laminate with uncracked plies above the midsurface but with microcracking in the plies below. Because the stiffness becomes that of either uncracked or cracked laminate, as determined by the local crack-opening/closure status, it is clear that the response of the cracked laminate can become nonlinear. For instance, when the laminate is subjected to shear loads at two different locations as shown in Fig. 2c, its behavior cannot be obtained by simply superimposing the separate responses obtained under the individual loadings shown in Figs. 2a and 2b, respectively. Behavior of this nonlinear nature is almost certain to be encountered if the cracked laminate deforms or vibrates about its undeformed position in which all cracks are just closed. In practice, it is more likely that the cracked laminate will be in a statically loaded configuration, which involves crack openings or closures at different locations as an initial condition before any further load is applied. Then the applied load may or may not lead to a nonlinear bimodular deformation, depending on the strain level associated with the load. Examples are shown in Figs. 3a–3c. In this paper, we deal with cracked laminates that vibrate around the flat position with small amplitude (Fig. 3b) and hence exhibit the nonlinear bimodular behavior.

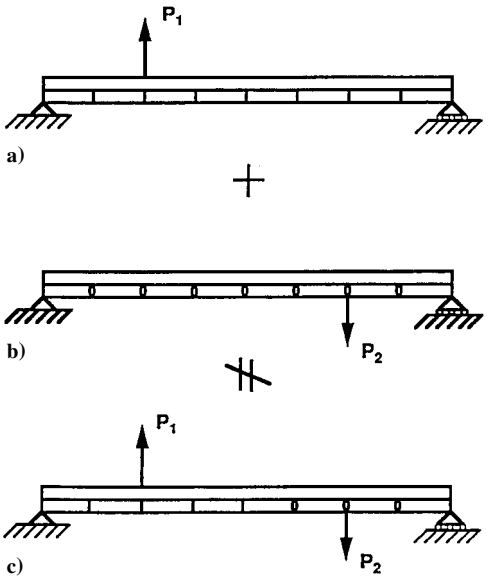

Fig. 2 Nonlinear bimodular deflection of a microcracked laminate under vertical shear loads.

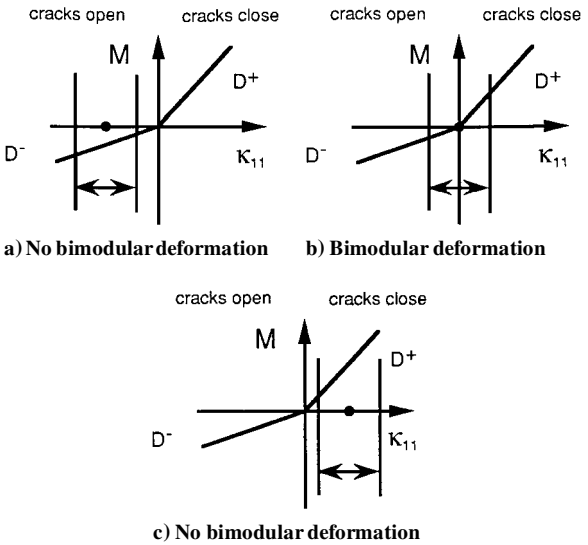

Fig. 3 Regions of different deformations on a bimodular moment-curvature curve.

V. Nonlinear Supersonic Flutter

Consider a two-dimensional laminated plate that is simply supported at both ends (Fig. 4). It is assumed that the plate is infinite in its transverse direction and the airflow outside is supersonic. No in-plane axial load is considered, as indicated earlier. We consider all microcracks to be in the plies below the neutral axis of the plate. To derive equations of motion, we assume that a thin-plate theory with Kirchhoff hypothesis can accurately yield the strain energy of the laminate. It is also assumed that the plate has negligible kinetic energy associated with the axial displacement u and

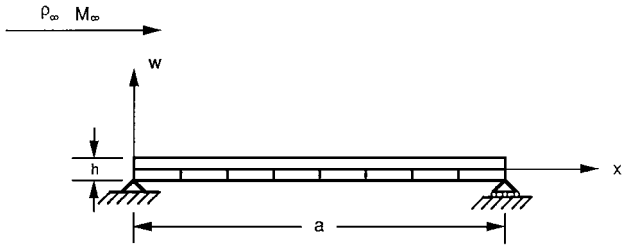

Fig. 4 Two-dimensional orthotropic panel in supersonic flow.

crack-opening/closure motion. Thus, one obtains equations of motion for small, geometrically linear deformations in the form

$$A(x,t)\frac{\partial^2 u}{\partial x^2} - B(x,t)\frac{\partial^3 w}{\partial x^3} = 0 \tag{25}$$

$$D(x,t)\frac{\partial^4 w}{\partial x^4} - B(x,t)\frac{\partial^3 u}{\partial x^3} + m\frac{\partial^2 w}{\partial t^2} + \Delta p(x,t) = 0 \tag{26}$$

where A and D are extensional and bending stiffness and B is the bending-extension coupling term. From the linear quasisteady theory, the aerodynamic pressure differential across the panel is (for $M_\infty > 1.6$) (Ref. 18)

$$\Delta p(x,t) = \frac{\rho_\infty U_\infty^2}{\sqrt{M_\infty^2 - 1}}\left(\frac{\partial w}{\partial x} + \frac{M_\infty^2 - 2}{M_\infty^2 - 1}\cdot\frac{1}{U_\infty}\cdot\frac{\partial w}{\partial t}\right) \tag{27}$$

In the present study, we do not consider formation of new microcracks during oscillations. Such may actually occur once a dynamic instability is encountered but is beyond the scope of this study. Instead, we concentrate on the initiation of flutter. Therefore, the stiffness coefficients will vary with time and space according to the crack-opening criterion discussed in a preceding section.

For the case of a cross-ply laminate with cracked plies in the 90-deg direction, Eq. (24) can be approximated as

$$\tilde{\epsilon}_{22}^{c\,90^\circ} \simeq \bar{\beta}\Lambda_{22}\left(L_{22}^{90^\circ} - \frac{L_{23}^{90^\circ 2}}{L_{33}^{90^\circ}}\right)\tilde{\epsilon}_{22}^{90^\circ}$$

$$= \bar{\beta}\Lambda_{22}\left(L_{22}^{90^\circ} - \frac{L_{23}^{90^\circ 2}}{L_{33}^{90^\circ}}\right)\left(-\frac{B}{A} + z^{90^\circ}\right)\kappa_{11} \tag{28}$$

It can be shown that, for our case, Λ^{22} and $L_{22}^{90^\circ} - (L_{23}^{90^\circ 2}/L_{33}^{90^\circ})$ are always positive. Also, when cracks are open, $-(B/A) + z^{90^\circ} < 0$. Thus, cracks will open if $\kappa_{11} < 0$ and will close if $\kappa_{11} > 0$. Accordingly, the stiffness coefficients vary as follows:

$$A(x,t) = \begin{Bmatrix} A^+;\ \kappa_{11} > 0 \\ A^-;\ \kappa_{11} < 0 \end{Bmatrix} \tag{29}$$

$$B(x,t) = \begin{Bmatrix} B^+(=0);\ \kappa_{11} > 0 \\ B^-;\ \kappa_{11} < 0 \end{Bmatrix} \tag{30}$$

$$D(x,t) = \begin{Bmatrix} D^+;\ \kappa_{11} > 0 \\ D^-;\ \kappa_{11} < 0 \end{Bmatrix} \tag{31}$$

Here the superscripts $\pm$ denote uncracked and cracked states, respectively. If an in-plane axial force exists, or if the plate undergoes large deflections during the oscillation, ascertaining crack-opening/closure states will be nontrivial.

In a nondimensional form, Eqs. (25) and (26) are reduced to the following single equation:

$$\left(1 - \frac{b^{\pm 2}}{a^\pm}\right)\frac{\partial^4 \bar{w}}{\partial \xi^4} + \lambda^\pm\frac{\partial \bar{w}}{\partial \xi} + g^\pm\frac{\partial^2 \bar{w}}{\partial \tau^2} + \lambda^\pm\gamma\frac{\partial \bar{w}}{\partial \tau} = 0 \tag{32}$$

where

$$a^\pm \equiv \frac{A^\pm a^4}{D^\pm h^2}, \qquad g^\pm \equiv \frac{D_0}{D^\pm}, \qquad b^\pm \equiv \frac{B^\pm a^2}{D^\pm h}$$

$$\lambda^\pm \equiv \frac{\rho_\infty U_\infty^2 a^3}{D^\pm\sqrt{M_\infty^2 - 1}}, \qquad \gamma \equiv \sqrt{\frac{\mu}{\lambda_0 M_\infty}}\left(\mu \equiv \frac{\rho_\infty a}{m}\right) \tag{33}$$

$$\tau \equiv t\sqrt{\frac{D_0}{ma^4}} \qquad (M_\infty \gg 1)$$

VI. Methods of Solution

A. Finite Difference Method

One can employ the central difference (explicit) or Newmark's (implicit) scheme for the time derivatives $\ddot{\bar{w}}$ and $\dot{\bar{w}}$ in the governing equation (32). For the $(n+1)$th step in time, Eq. (32) can be written in the first-order form in space as

$$\frac{\partial \boldsymbol{Y}_{n+1}}{\partial \xi} = \boldsymbol{A}^\pm \boldsymbol{Y}_n + \boldsymbol{U}_n \tag{34}$$

where

$$\boldsymbol{Y} = \lfloor y_1 \quad y_2 \quad y_3 \quad y_4 \rfloor^T \equiv \lfloor \bar{w} \quad \bar{w}' \quad \bar{w}'' \quad \bar{w}''' \rfloor^T$$

When using Newmark's scheme,[19] the system matrix $\boldsymbol{A}^\pm$ and the input vector $\boldsymbol{U}_n$ are defined as

$$\boldsymbol{A}^\pm = \begin{bmatrix} 0 & 1 & 0 & 0 \\ 0 & 0 & 1 & 0 \\ 0 & 0 & 0 & 1 \\ b_1^\pm & b_2^\pm & 0 & 0 \end{bmatrix}, \qquad \boldsymbol{U}_n = \begin{Bmatrix} 0 \\ 0 \\ 0 \\ b_3^\pm y_{1n} + b_4^\pm \dot{y}_{1n} + b_5^\pm \ddot{y}_{1n} \end{Bmatrix} \tag{35}$$

where

$$b_1^\pm = -\frac{\bar{g}^\pm}{\beta(\Delta\tau)^2} - \bar{\lambda}^\pm\gamma\frac{\lambda}{\beta\Delta\tau}, \qquad b_2^\pm = -\bar{\lambda}^\pm \tag{36}$$

$$b_3^\pm = -b_1^\pm, \qquad b_4^\pm = (\bar{g}^\pm/\beta\Delta\tau) - \bar{\lambda}^\pm\gamma[1 - (\lambda/\beta)] \tag{37}$$

$$b_5^\pm = \bar{g}^\pm[(1/2\beta) - 1] - \bar{\lambda}^\pm\gamma[1 - (\lambda/2\beta)]\Delta\tau \tag{38}$$

and

$$\bar{g}^\pm \equiv \frac{g^\pm}{1 - (b^{\pm 2}/a^\pm)} \tag{39}$$

$$\bar{\lambda}^\pm \equiv \frac{\lambda^\pm}{1 - (b^{\pm 2}/a^\pm)} \tag{40}$$

The boundary conditions at both ends of the laminate are (for all n)

$$y_{1n}(\xi = 0) = y_{1n}(\xi = 1) = 0 \tag{41}$$

$$y_{3n}(\xi = 0) = y_{3n}(\xi = 1) = 0 \tag{42}$$

The initial conditions are given as

$$y_{10}(\xi) = \bar{w}_0(\xi) \tag{43}$$

$$\dot{y}_{10}(\xi) = \dot{\bar{w}}_0(\xi) \tag{44}$$

$$\ddot{y}_{10}(\xi) = -\frac{1}{\bar{g}^\pm(\bar{w}_0'')}\left[\bar{w}_0'''' + \bar{\lambda}^\pm(\bar{w}_0'')\bar{w}_0' + \bar{\lambda}^\pm(\bar{w}_0'')\gamma\dot{\bar{w}}_0\right] \tag{45}$$

To solve the nonlinear system shown in Eq. (34), the following steps are repeated at each time step $(n+1)\cdot\Delta\tau$.

1) Assume $y_{2(n+1)}$ and $y_{4(n+1)}$ at $\xi = 0$.
2) Integrate from $\xi = 0$ to $\xi = 1$.
3) At $\xi = 1$, check if $y_{1(n+1)} \approx 0$ and if $y_{3(n+1)} \approx 0$.
4) If not, formulate and perform a Newton–Raphson iteration until satisfied.
5) Calculate $\dot{y}_{1(n+1)}$ and $\ddot{y}_{1(n+1)}$.

At each node, the proper $\bar{g}^\pm$ and $\bar{\lambda}^\pm$, according to the sign of $y_{3(n+1)}$ (curvature), must be used.

B. Finite Element Method

Suppose that the plate is divided into M elements of equal length $\bar{l}$. It is assumed that the crack-opening/closure state is piecewise constant within each element. That is, cracks in each element are assumed to be either all open or all closed, based on the average curvature of the element. Expressing total strain, kinetic energy, and work in terms of the nondimensional variables and parameters defined in the preceding sections, the Hamilton principle equation can be written as

$$\delta\int_{\tau_1}^{\tau_2}\sum_1^M \frac{1}{2}\int_0^{\bar{l}}\left(\frac{\partial^2\bar{w}}{\partial\xi^2}\right)^2 \mathrm{d}\xi\,\mathrm{d}\tau + \delta\int_{\tau_1}^{\tau_2}\sum_1^M \frac{a^{\pm}}{2}\int_0^{\bar{l}}\left(\frac{\partial\bar{u}}{\partial\xi}\right)^2 \mathrm{d}\xi\,\mathrm{d}\tau$$
$$- \delta\int_{\tau_1}^{\tau_2}\sum_1^M b^{\pm}\int_0^{\bar{l}}\frac{\partial\bar{u}}{\partial\xi}\frac{\partial^2\bar{w}}{\partial\xi^2}\,\mathrm{d}\xi\,\mathrm{d}\tau$$
$$- \delta\int_{\tau_1}^{\tau_2}\sum_1^M \frac{1}{2}\int_0^{\bar{l}} g^{\pm}\left(\frac{\partial\bar{w}}{\partial\tau}\right)^2 \mathrm{d}\xi\,\mathrm{d}\tau$$
$$+ \int_{\tau_1}^{\tau_2}\sum_1^M \int_0^{\bar{l}} \lambda^{\pm}\left(\frac{\partial\bar{w}}{\partial\xi} + \gamma\frac{\partial\bar{w}}{\partial\tau}\right)\delta\bar{w}\,\mathrm{d}\xi\,\mathrm{d}\tau = 0 \tag{46}$$

The displacement field is expressed in terms of shape functions and nodal displacements:

$$\begin{Bmatrix}\bar{u}\\ \bar{w}\end{Bmatrix} = \boldsymbol{N}\boldsymbol{d} \tag{47}$$

where $\boldsymbol{d} \equiv [u_1\ \ w_1\ \ w_1'\ \ u_2\ \ w_2\ \ w_2']^T$ and

$$\boldsymbol{N} \equiv \begin{bmatrix} N_{u1} & 0 & 0 & N_{u2} & 0 & 0\\ 0 & N_{w1} & N_{w2} & 0 & N_{w3} & N_{w4}\end{bmatrix} \tag{48}$$

In the preceding, linear and cubic Hermitian polynomials are used for $\bar{u}$ and $\bar{w}$, respectively.[19] The vector $\boldsymbol{d}$ contains three nodal displacements $(\bar{u},\ \bar{w},\ \bar{w}')$ at each end of an element. Defining the strain field vector $\boldsymbol{B}_u$ and $\boldsymbol{B}_w$ as

$$\boldsymbol{B}_u \equiv \begin{bmatrix}\dfrac{\mathrm{d}N_{u1}}{\mathrm{d}\xi} & 0 & 0 & \dfrac{\mathrm{d}N_{u2}}{\mathrm{d}\xi} & 0 & 0\end{bmatrix} \tag{49}$$

$$\boldsymbol{B}_w \equiv \begin{bmatrix}0 & \dfrac{\mathrm{d}^2N_{w1}}{\mathrm{d}\xi^2} & \dfrac{\mathrm{d}^2N_{w2}}{\mathrm{d}\xi^2} & 0 & \dfrac{\mathrm{d}^2N_{w3}}{\mathrm{d}\xi^2} & \dfrac{\mathrm{d}^2N_{w4}}{\mathrm{d}\xi^2}\end{bmatrix} \tag{50}$$

leads to the global assembled equation

$$\boldsymbol{M}\ddot{\boldsymbol{D}} + \boldsymbol{C}\dot{\boldsymbol{D}} + \boldsymbol{K}\boldsymbol{D} = 0 \tag{51}$$

where

$$\boldsymbol{M} \equiv \sum_1^M g^{\pm}\boldsymbol{m} \tag{52}$$

$$\boldsymbol{C} \equiv \gamma\sum_1^M \lambda^{\pm}\boldsymbol{m} \tag{53}$$

$$\boldsymbol{K} \equiv \sum_1^M (\boldsymbol{k}^{\pm} + \lambda^{\pm}\boldsymbol{a}) \tag{54}$$

$$\boldsymbol{m} \equiv \int_0^{\bar{l}} \boldsymbol{N}_2^T\boldsymbol{N}_2\,\mathrm{d}\xi \tag{55}$$

$$\boldsymbol{k}^{\pm} \equiv \int_0^{\bar{l}} \left(\boldsymbol{B}_w^T\boldsymbol{B}_w + a^{\pm}\boldsymbol{B}_u^T\boldsymbol{B}_u - b^{\pm}\boldsymbol{B}_u^T\boldsymbol{B}_w - b^{\pm}\boldsymbol{B}_w^T\boldsymbol{B}_u\right)\mathrm{d}\xi \tag{56}$$

$$\boldsymbol{a} \equiv \int_0^{\bar{l}} \boldsymbol{N}_2^T\frac{\mathrm{d}\boldsymbol{N}_2}{\mathrm{d}\xi}\,\mathrm{d}\xi \tag{57}$$

Employing Newmark's scheme at $(n+1)\cdot\Delta\tau$,

$$\hat{\boldsymbol{K}}_{n+1}\boldsymbol{D}_{n+1} = \boldsymbol{R}_{n+1} \tag{58}$$

where

$$\hat{\boldsymbol{K}}_{n+1} = \boldsymbol{K}_{n+1} + \frac{1}{\beta(\Delta\tau)^2}\boldsymbol{M}_{n+1} + \frac{\lambda}{\beta\Delta\tau}\boldsymbol{C}_{n+1} \tag{59}$$

$$\boldsymbol{R}_{n+1} = \boldsymbol{M}_{n+1}\left[\frac{1}{\beta(\Delta\tau)^2}\boldsymbol{D}_n + \frac{1}{\beta\Delta\tau}\dot{\boldsymbol{D}}_n + \left(\frac{1}{2\beta} - 1\right)\ddot{\boldsymbol{D}}_n\right]$$
$$+ \boldsymbol{C}_{n+1}\left[\frac{\lambda}{\beta\Delta\tau}\boldsymbol{D}_n + \left(\frac{\lambda}{\beta} - 1\right)\dot{\boldsymbol{D}}_n + \Delta\tau\left(\frac{\lambda}{2\beta} - 1\right)\ddot{\boldsymbol{D}}_n\right] \tag{60}$$

At each time step, the following iteration is performed.

1) Set

$$\boldsymbol{M}_{n+1}^{(0)} = \boldsymbol{M}_n, \qquad \boldsymbol{C}_{n+1}^{(0)} = \boldsymbol{C}_n, \qquad \boldsymbol{K}_{n+1}^{(0)} = \boldsymbol{K}_n$$

and solve

$$\boldsymbol{D}_{n+1}^{(1)} = \hat{\boldsymbol{K}}_{n+1}^{(0)^{-1}}\boldsymbol{R}_{n+1}^{(0)}$$

.

2) Repeat

$$\boldsymbol{D}_{n+1}^{(i+1)} = \hat{\boldsymbol{K}}_{n+1}^{(i)^{-1}}\boldsymbol{R}_{n+1}^{(i)} \qquad \text{until} \qquad \left\|\boldsymbol{D}_{n+1}^{(i+1)} - \boldsymbol{D}_{n+1}^{(i)}\right\| \ll 1$$

where

$$\hat{\boldsymbol{K}}_{n+1}^{(i)} = \hat{\boldsymbol{K}}_{n+1}\left[\boldsymbol{D}_{n+1}^{(i)}\right]$$
$$\boldsymbol{R}_{n+1}^{(i)} = \boldsymbol{R}_{n+1}\left[\boldsymbol{D}_{n+1}^{(i)}\right]$$

Usually, only a few interations are needed at each time step. As mentioned earlier, the crack opening or closure in each element is determined by the sign of the averaged curvature of the element.

Although the methods of solution described so far include the effect of bending-extension coupling due to microcracks, this effect can be ignored for practical purposes. Indeed, in all of the numerical examples to follow, the magnitudes of nonzero B_{ij} are found to be negligible compared with those of A_{ij} and D_{ij}. Hence, $b^{\pm} \simeq 0$, $\bar{g}^{\pm} \simeq g^{\pm}$, $\bar{\lambda}^{\pm} \simeq \lambda^{\pm}$, and the axial displacement u can be ignored. The finite element formulation for this case simplifies significantly. The resulting new formulation is not shown here.

VII. Results and Discussion

A. Reduced Stiffness of Cross- and Angle-Ply Laminates

In the first part of this section, we present reduced-stiffness results for several symmetric composite laminates under different loading conditions. The undamaged uniply properties are those of VS0054 graphite/epoxy ($\nu_f = 0.2$ and $\nu_m = 0.8$) given in Ref. 7. Our purpose is to examine, in qualitative terms, the overall changes in the stiffness and compliance of the laminates due to microcracking. We do not intend here an extensive parametric study for a wide variety of crack densities in various plies. Instead, we concentrate on one particular density value, $\beta = 1$. (This applies to interior cracked plies. For an outer cracked ply, the effective crack density becomes $\beta = 2$.)

The first group of laminates considered are $[0/90]_s$ and $[90/0]_s$ cross-ply laminates under the one-dimensional bending moment M_{11}. The microcracks have been introduced only in the 90-deg plies below the midsurface (Figs. 5 and 6). Listed next are the $\boldsymbol{A}$, $\boldsymbol{B}$, and $\boldsymbol{D}$ matrices for $\beta = 1$ as obtained using Eqs. (14–16). Also presented are new neutral axis locations z_n expressed in terms of a fraction of the uniply thickness t. As expected, when microcracks exist in the

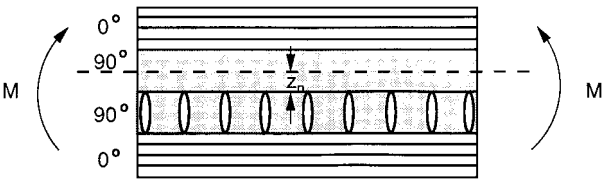

Fig. 5 Crack opening of a $[0/90]_s$ laminate.

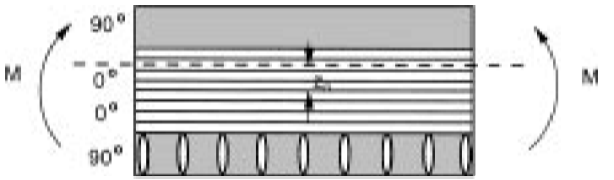

Fig. 6 Crack opening of a $[90/0]_s$ laminate.

90-deg layers only, the transverse modulus A_{22} changes very little. However, there are significant reductions in other moduli in both the $[0/90]_s$ and $[90/0]_s$ laminates. Of particular interest are decreases in the bending stiffness D_{11} and the torsional stiffness D_{66}. Furthermore, new bending-extension couplings in the matrix $\boldsymbol{B}$ are now present in the case of cracked laminates. The reduction in the bending stiffness D_{11} is more prominent for the $[90/0]_s$ laminate because the cracked 90-deg ply is located farther from the neutral axis than in the $[0/90]_s$ laminate. Both cross-ply laminates will exhibit the nonlinear bimodular deformation when bent about undeformed, flat positions.

$[0/90]_s$ (uncracked):

$$\boldsymbol{A}_0 = \begin{bmatrix} 40.69 & 2.21 & 0 \\ & 40.69 & 0 \\ \text{(Symm)} & & 1.04 \end{bmatrix} \text{(MN/m)}$$

$$\boldsymbol{D}_0 = \begin{bmatrix} 1.661 & 0.054 & 0 \\ & 0.317 & 0 \\ \text{(Symm)} & & 0.025 \end{bmatrix} \text{(N-m)}$$

$$\boldsymbol{B}_0 = 0, \qquad z_n = 0$$

$[0/90]_s$ (cracked) (0.8% reduction in D_{11}):

$$\boldsymbol{A}_c = \begin{bmatrix} 40.373 & 1.664 & 0 \\ & 39.742 & 0 \\ \text{(Symm)} & & 0.841 \end{bmatrix} \text{(MN/m)}$$

$$\boldsymbol{D}_c = \begin{bmatrix} 1.647 & 0.031 & 0 \\ & 0.277 & 0 \\ \text{(Symm)} & & 0.017 \end{bmatrix} \text{(N-m)}$$

$$\boldsymbol{B}_c = \begin{bmatrix} 0.064 & 0.111 & 0 \\ & 0.192 & 0 \\ \text{(Symm)} & & 0.040 \end{bmatrix} \text{(kN)}, \qquad z_n = 0.012t$$

$[90/0]_s$ (uncracked):

$$\boldsymbol{A}_0 = \begin{bmatrix} 40.69 & 2.21 & 0 \\ & 40.69 & 0 \\ \text{(Symm)} & & 1.04 \end{bmatrix} \text{(MN/m)}$$

$$\boldsymbol{D}_0 = \begin{bmatrix} 0.317 & 0.054 & 0 \\ & 1.661 & 0 \\ \text{(Symm)} & & 0.025 \end{bmatrix} \text{(kN)}$$

$$\boldsymbol{B}_0 = 0, \qquad z_n = 0$$

$[90/0]_s$ (cracked) (12.7% reduction in D_{11}):

$$\boldsymbol{A}_c = \begin{bmatrix} 39.742 & 1.664 & 0 \\ & 40.373 & 0 \\ \text{(Symm)} & & 0.841 \end{bmatrix} \text{(MN/m)}$$

$$\boldsymbol{D}_c = \begin{bmatrix} 0.277 & 0.031 & 0 \\ & 1.647 & 0 \\ \text{(Symm)} & & 0.017 \end{bmatrix} \text{(N-m)}$$

$$\boldsymbol{B}_c = \begin{bmatrix} 0.192 & 0.111 & 0 \\ & 0.064 & 0 \\ \text{(Symm)} & & 0.040 \end{bmatrix} \text{(kN)}, \qquad z_n = 0.036t$$

The next case is that of the angle-ply laminate $[\pm 45]_s$ subjected to the twisting moment M_{12}. When used for a lifting surface, this laminate will have the beneficial bending-torsion elastic coupling or the so-called washout effect that can be useful in aeroelastic tailoring. It can be shown that, when plies below the midsurface are cracked, all microcracks will close for $M_{12} < 0$ and open for $M_{12} > 0$ (Fig. 7). In the following, along with the reduced stiffness, we show estimated percentage changes in the compliance matrices.

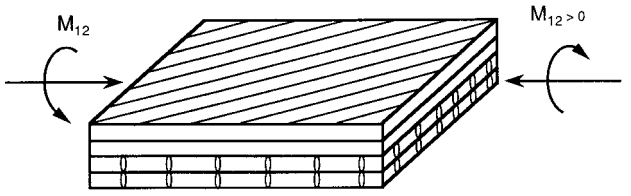

Fig. 7 Crack opening of a $[\pm 45]_s$ laminate.

It is seen that both bending and torsion compliances of the cracked laminate will increase, whereas the bending-torsion coupling will decrease. Hence, the degradation of aeroelastic stability could be serious if such a laminate is designed for use in a lifting surface.

$[\pm 45]_s$ (uncracked):

$$\boldsymbol{A}_0 = \begin{bmatrix} 22.490 & 20.411 & 0 \\ & 22.490 & 0 \\ \text{(Symm)} & & 19.239 \end{bmatrix} \text{(MN/m)}$$

$$\boldsymbol{D}_0 = \begin{bmatrix} 0.547 & 0.496 & 0.336 \\ & 0.547 & 0.336 \\ \text{(Symm)} & & 0.468 \end{bmatrix} \text{(N-m)}, \qquad \boldsymbol{B}_0 = 0$$

$[\pm 45]_s$ (cracked), for $M_{12} < 0$, all cracks close, and for $M_{12} > 0$, all cracks open:

$$\boldsymbol{A}_c = \begin{bmatrix} 21.017 & 19.614 & 0.012 \\ & 21.017 & 0.012 \\ \text{(Symm)} & & 19.158 \end{bmatrix} \text{(MN/m)}$$

$$\boldsymbol{D}_c = \begin{bmatrix} 0.509 & 0.477 & 0.342 \\ & 0.509 & 0.342 \\ \text{(Symm)} & & 0.466 \end{bmatrix} \text{(N-m)}$$

$$\boldsymbol{B}_c = \begin{bmatrix} 0.206 & 0.107 & -0.022 \\ & 0.206 & -0.022 \\ \text{(Symm)} & & 0.011 \end{bmatrix} \text{(kN)}$$

Percentage changes in the compliance matrix $\boldsymbol{D}^{-1}$:

$$\boldsymbol{D}_0^{-1} = \begin{bmatrix} 10.7904 & -9.0040 & -1.2835 \\ & 10.7904 & -1.2835 \\ \text{(Symm)} & & 3.9835 \end{bmatrix} \text{(1/Pa)}$$

$$\boldsymbol{D}_c^{-1} = \begin{bmatrix} 21.0821 & -19.0028 & -1.5275 \\ & 21.0821 & -1.5275 \\ \text{(Symm)} & & 4.3926 \end{bmatrix} \text{(1/Pa)}$$

Increase in the bending compliance:

$$\frac{D_{c11}^{-1}}{D_{011}^{-1}} \approx 195\%$$

Increase in the torsion compliance:

$$\frac{D_{c66}^{-1}}{D_{066}^{-1}} \approx 110\%$$

Reduction in the bending-torsion coupling:

$$\frac{D_{c16}^{-1}/D_{c11}^{-1}}{D_{016}^{-1}/D_{011}^{-1}} \approx 60.9\%$$

The observations and conclusions drawn in this section should not be restricted to graphite/epoxy laminates. In other words, depending on the fiber and matrix materials used and their volume fractions, the extent to which the matrix cracks affect various laminate moduli can be quite significant. Therefore, an appropriate investigation must be conducted to adequately define the impact of the microcracking.

B. Free Vibration Results

In the second part of this section, nonlinear bimodular free-vibration responses of the microcracked composite laminates that

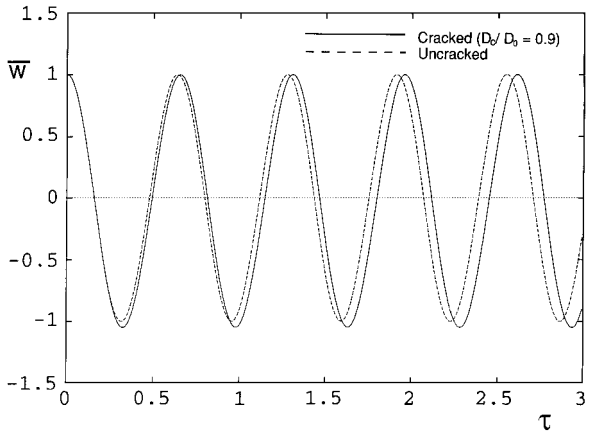

Fig. 8 Free vibration responses at $\xi = 0.5$ subjected to initial displacement $\sin(\pi\xi)$.

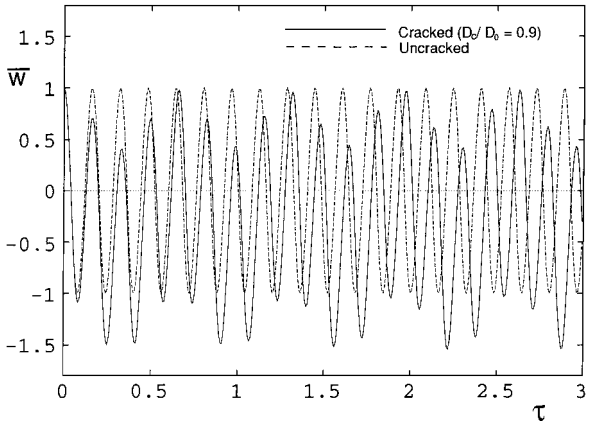

Fig. 9 Free vibration responses at $\xi = 0.25$ subjected to initial displacement $\sin(2\pi\xi)$.

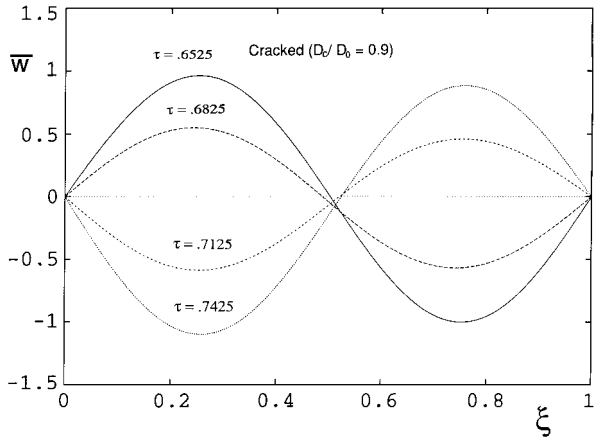

Fig. 10 Free vibration modes during a half-cycle subjected to initial displacement $\sin(2\pi\xi)$.

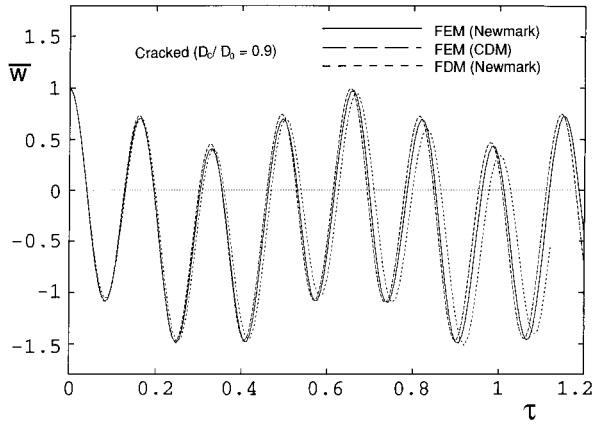

Fig. 11 Free vibration responses at $\xi = 0.25$ subjected to initial displacement $\sin(2\pi\xi)$ using different methods.

are infinite in their transverse direction are presented. Because the plates are two dimensional, the longitudinal flexural rigidity D_{11} determines the characteristics of the vibration. Hence, without loss of generality the analysis is limited to the symmetric cross ply $[0/90]_s$. Unless indicated otherwise, all results were obtained using eight Hermitian finite elements and Newmark's integration scheme with $\lambda = 0.5$ and $\beta = 0.4$. Longitudinal motion due to bending-extension coupling was ignored.

Figure 8 shows free vibration responses vs time at the midpoint of both the uncracked and cracked plates. It is assumed that the cracked laminate has a bending stiffness that is 10% smaller than that of the uncracked one. The initial deflection is given in the form of $\sin(\pi\xi)$, i.e., the first vibration mode of the uncracked plate. In this position, all of the cracks are initially closed. Hence, the plate starts to vibrate with the uncracked stiffness D_0. After the first quarter of its first cycle, the cracked plate assumes an exact flat position in which all cracks are about to open. The plate then moves down with the reduced stiffness D_c, and after a half-cycle it resumes the flat position. For the remainder of the cycle, the plate moves with D_0. The subsequent motion of the cracked plate repeats its first cycle. This response has a characteristic similar to that of a prismatic bar with bimodular longitudinal stiffness.[20] From Fig. 8, it can be seen that the period shifting resulted from the bimodular motion. Also, the maximum peak on the negative side is greater than its counterpart on the positive side. The oscillation shown in Fig. 8 should not be termed nonlinear because each half-period of the motion can be completely predicted by linear analysis.

If the initial disturbance displacement is chosen as the second mode $\sin(2\pi\xi)$, however, the motion of the cracked plate is quite different, as shown in Fig. 9. Here, there no longer exists smooth shift of motion between the cracked and uncracked plates as crack opening/closure is not uniform along the plate at any instant of motion. The motion is indeed nonlinear bimodular. Figure 10 shows the free-vibration-mode shapes at different instants during a half-cycle subjected to the same initial condition. Because of the nonlinear nature of this oscillation, the mode shapes do not exactly concur at the midpoint. In fact, the location of the node point oscillates. Figures 9 and 10 also indicate that the maximum amplitude level shifts from one part of a cycle to another. Figure 11 represents responses obtained using different methods. To obtain convergence in the finite difference result, it was necessary to put more than 1000 nodes along the plate. For the finite difference result, the time increment of $\Delta\tau = 2.0 \times 10^{-2}$ was used. For the finite element results, 20 elements with $\Delta\tau = 0.75 \times 10^{-2}$ for the Newmark method and 12 elements with $\Delta\tau = 0.25 \times 10^{-2}$ for the central difference method were used. Both the finite element and finite difference methods seem to converge well. However, the finite difference method requires much longer computing time because of the large number of nodes required. Figure 12 shows the results of a convergence study using a different number of finite elements for the same cracked plate. The free vibration displacements are plotted for four such element numbers. Eight elements give results with sufficient accuracy (Fig. 12).

C. Flutter Responses and Stability Results

In this section, the nonlinear bimodular flutter response of the cracked cross-ply laminates considered in the preceding section is explored. All of the responses are subjected to the initial displacement $\sin(\pi\xi)$.

In Fig. 13, panel flutter responses for both cracked and uncracked cross-ply laminates are plotted at $\lambda = 303$. In both cases, aerodynamic damping is sufficiently dominant to damp out the initial disturbances. However, at $\lambda = 328.5$, the cracked laminate becomes neutrally unstable (Fig. 14), whereas the uncracked laminate has not yet reached its flutter point. Figure 15 shows flutter mode shapes of the cracked laminate during a half-cycle of the motion at the critical

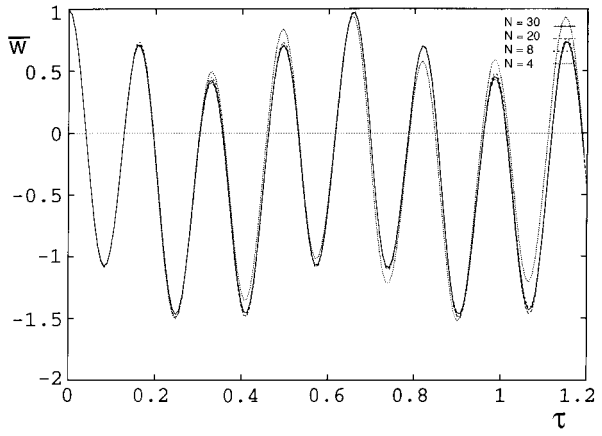

Fig. 12 Convergence of finite element solutions for free vibration responses subjected to initial displacement $\sin(2\pi\xi)$.

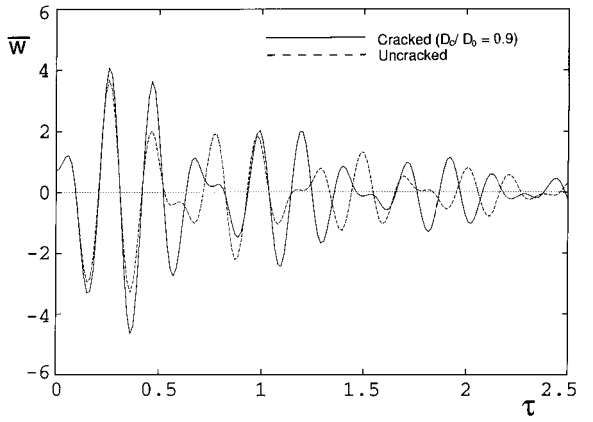

Fig. 13 Flutter responses at $\xi = 0.75$ at a preflutter point (μ/M = 0.01, D_c/D_0 = 0.9, and λ = 303).

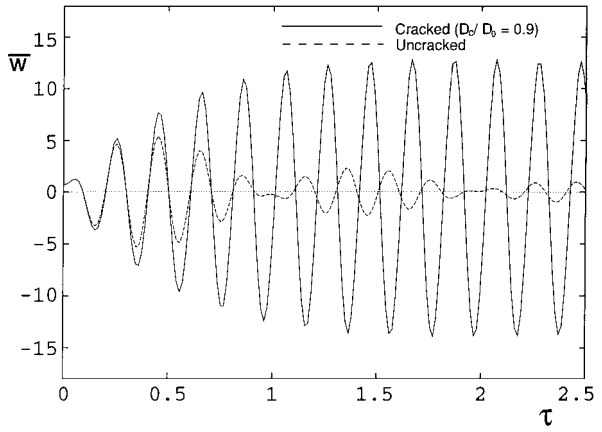

Fig. 14 Flutter responses at ξ = 0.75 at the critical flutter point (μ/M = 0.01, D_c/D_0 = 0.9, and λ_{cr} = 328.5).

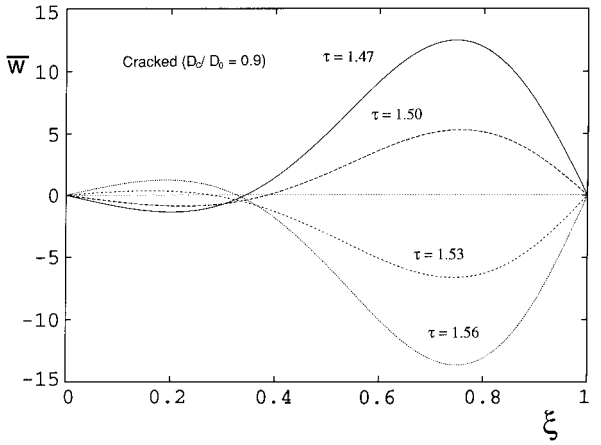

Fig. 15 Flutter modes at the critical flutter point (μ/M = 0.01, D_c/D_0 = 0.9, and λ_{cr} = 328.5).

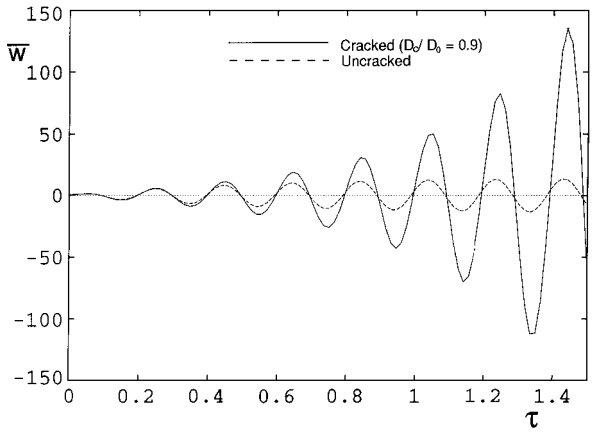

Fig. 16 Flutter responses at $\xi = 0.75$ at a postflutter point (μ/M = 0.01, D_c/D_0 = 0.9, and λ = 344.4).

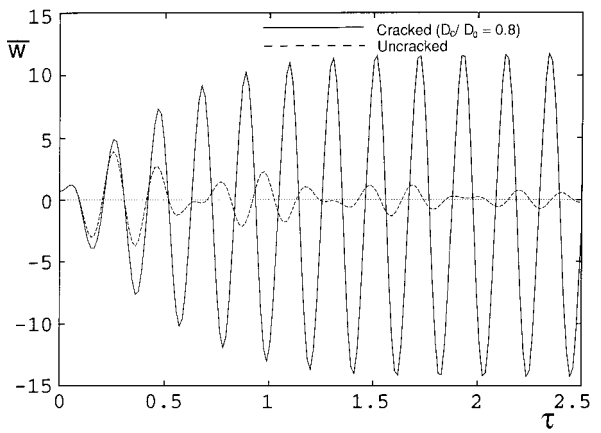

Fig. 17 Flutter responses at ξ = 0.75 at the critical flutter point (μ/M = 0.01, D_c/D_0 = 0.8, and λ_{cr} = 309.2).

speed. This flutter mode shape resembles that of the uncracked plate. Note that the maximum amplitude occurs at around $\xi = 0.75$. But the peak amplitude for $\bar{w} < 0$ is greater than that for $\bar{w} > 0$, as a result of the bimodular oscillation. The effects of nonlinearity, however, do not seem profound because the dominant mode shape is that of the first vibration mode. It should also be emphasized that, for a given set of parameters, the limit cycle amplitude and frequency are independent of the form of initial conditions. Figure 16 shows a postflutter response at $\lambda = 344.4$, which is the flutter boundary for the uncracked laminate. Concerning the cracked laminate behavior in Fig. 14 and the uncracked laminate behavior in Fig. 16, it appears that a 10% reduction in the bending modulus has resulted in about a 5% reduction in the critical dynamic pressure. As might be expected, then, if the stiffness decreases by 20%, the critical dynamic pressure could drop about 10%, as shown in Fig. 17. It appears thus that flutter stability of a two-dimensional microcracked laminate as indicated by critical dynamic pressure will be reduced as much as half of the percentage reduction in the bending stiffness.

VIII. Conclusion

In this study, a finite difference and a finite element model of microcracked composite plates undergoing two-dimensional nonlinear bimodular flutter oscillations have been presented using a two-phase, self-consistent crack model and quasisteady supersonic aerodynamic loads. When the microcracked plate deforms about its static configuration in a nonlinear fashion, it is referred to as nonlinear bimodular deformation. As this was a preliminary investigation of such a phenomenon, no attempt has been made to deal with layups

that are used in actual structures. Numerical simulations in the time domain showed that, for the two-dimensional flutter problem, microcracks in composites cause reduced aeroelastic stability through a direct reduction in the bending stiffness and nonlinear bimodular oscillation. However, stiffness results of an angle-ply laminate suggested that microcracking can degrade the aeroelastic stability further by reducing the torsional stiffness and bending-torsion coupling. Future investigations need to be focused on the influences of microcracking on elastic couplings as well as various stiffness terms and their potential impact on the aeroelastic performances of realistic composite structures.

Acknowledgments

The support of this work by the Air Force Office of Scientific Research, with Spencer Wu as the Program Official, is gratefully acknowledged.

References

[1]Birman, V., and Librescu, L., "Supersonic Flutter of Shear Deformable Laminated Composite Flat Panels," *Journal of Sound and Vibration*, Vol. 139, No. 2, 1990, pp. 265–275.

[2]Ehlers, S. M., and Weisshaar, T. A., "Adaptive Wing Flexural Axis Control," *Proceedings of the Third International Conference on Adaptive Structures*, Technomic, Lancaster, PA, 1992, pp. 28–40.

[3]Abdelnaser, A. S., and Singh, M. P., "Forced and Random Vibrations of Composite Beams with Bending Torsion Coupling and General Boundary Conditions," *Proceedings of the AIAA/ASME/ASEE/AHS/ASC 34th Structures, Structural Dynamics, and Materials Conference*, AIAA, Washington, DC, 1993, pp. 683–692 (AIAA Paper 93-1375).

[4]Smith, E. C., "Vibration and Flutter of Stiff-Inplane Elastically Tailored Composite Rotor Blades," *Proceedings of the AIAA/ASME/ASEE/AHS/ASC 34th Structures, Structural Dynamics, and Materials Conference*, AIAA, Washington, DC, 1993, pp. 26–37 (AIAA Paper 93-1302).

[5]Smith, E. C., and Chopra, I., "Air and Ground Resonance of Helicopters with Elastically Tailored Composite Rotor Blades," *Journal of the American Helicopter Society*, Vol. 38, No. 4, 1993, pp. 50–61.

[6]Hill, S. C., "A Theory for Predicting and Minimizing the Effects of Matrix Degradation on the Thermomechanical Properties of General Laminates," Ph.D. Thesis, Dept. of Mechanical Engineering, Aeronautical Engineering and Mechanics, Rensselaer Polytechnic Inst., Troy, NY, Dec. 1993.

[7]Budiansky, B., and O'Connell, R. J., "Elastic Moduli of a Cracked Solid," *International Journal of Solids and Structures*, Vol. 12, No. 1, 1976, pp. 81–97.

[8]Laws, N., Dvorak, G. J., and Hejazi, M., "Stiffness Changes in Unidirectional Composites Caused by Crack Systems," *Mechanics of Materials*, Vol. 2, No. 2, 1983, pp. 123–137.

[9]Dvorak, G. J., Laws, N., and Hejazi, M., "Analysis of Progressive Matrix Cracking in Composite Laminates—I. Thermoelastic Properties of a Ply with Cracks," *Journal of Composite Materials*, Vol. 19, No. 3, 1985, pp. 216–234.

[10]Fu, Y., and Evans, A. G., "Some Effects of Microcracks on the Mechanical Properties of Brittle Solids—I. Stress, Strain Relations," *Acta Metallurgica*, Vol. 33, No. 8, 1985, pp. 1515–1523.

[11]Evans, A. G., and Fu, Y., "Some Effects of Microcracks on the Mechanical Properties of Brittle Solids—II. Microcrack Toughening," *Acta Metallurgica*, Vol. 33, No. 8, 1985, pp. 1525–1531.

[12]Toi, Y., and Atluri, S. N., "Finite Element Analysis of Static and Dynamic Fracture of Brittle Microcracking Solids," *International Journal of Plasticity*, Vol. 6, No. 2, 1990, pp. 169–188.

[13]Makins, R. K., and Adali, S., "Bending of Cross-Ply Laminated Plates with Matrix Cracks," *Journal of Strain Analysis*, Vol. 26, No. 4, 1991, pp. 253–257.

[14]Adali, S., and Makins, R. K., "Buckling of Unsymmetrical Cross-Ply Laminates with Matrix Cracks," *International Journal of Mechanical Sciences*, Vol. 33, No. 10, 1991, pp. 851–861.

[15]Adali, S., and Makins, R. K., "Effect of Transverse Matrix Cracks on the Frequencies of Unsymmetrical Cross-Ply Laminates," *Journal of Franklin Institute*, Vol. 329, No. 4, 1992, pp. 655–665.

[16]Horii, H., and Nemat-Nasser, S., "Overall Moduli of Solids with Microcracks: Load-Induced Anisotropy," *Journal of the Mechanics and Physics of Solids*, Vol. 31, No. 2, 1983, pp. 155–171.

[17]Jones, R. M., *Mechanics of Composite Materials*, McGraw–Hill, New York, 1975, Chap. 4.

[18]Dowell, E. H., "Nonlinear Oscillations of a Fluttering Plate," *AIAA Journal*, Vol. 4, No. 7, 1966, pp. 1267–1275.

[19]Bathe, K., *Finite Element Procedures in Engineering Analysis*, Prentice–Hall, New York, 1982, Chaps. 5 and 9.

[20]Khachatryan, A. A., "Longitudinal Vibrations of Prismatic Bars Made of Different-Modulus Materials," *Mekhanika Tverdogo Tela*, Vol. 2, No. 5, 1967, pp. 140–145.

R. K. Kapania
Associate Editor